ISSN 1027-4510, Journal of Surface Investigation. X-ray, Synchrotron and Neutron Techniques, 2014, Vol. 8, No. 2, pp. 220–228. © Pleiades Publishing, Ltd., 2014.
Original Russian Text © A.V. Bakaev, D.A. Terentyev, P.Yu. Grigorev, E.E. Zhurkin, 2014, published in Poverkhnost'. Rentgenovskie, Sinkhrotronnye i Neitronnye Issledovaniya, 2014, No. 3, pp. 24–33.

Atomistic Simulation of the Interaction between Mobile Edge Dislocations and Radiation-Induced Defects in Fe–Ni–Cr Austenitic Alloys

A. V. Bakaev[a, b], D. A. Terentyev[b], P. Yu. Grigorev[a, b], and E. E. Zhurkin[a]

[a] *St. Petersburg State Polytechnic University, St. Petersburg, Russia*
[b] *SCK-CEN, Belgian Nuclear Research Center, Mol, Belgium*

Received July 17, 2013

Abstract—The classical molecular dynamics method is employed to simulate the interaction of edge dislocations with interstitial Frank loops (2 and 5 nm in diameter) in the $Fe–Ni_{10}–Cr_{20}$ model alloy at the temperatures $T = 300–900$ K. The examined Frank loops are typical extended radiation-induced defects in austenitic steels adapted to nuclear reactors, while the chosen triple alloy ($Fe–Ni_{10}–Cr_{20}$) has the alloying element concentration maximally resembling these steels. The dislocation–defect interaction mechanisms are ascertained and classified, and their comparison with the previously published data concerning screw dislocations is carried out. The detachment stress needed for a dislocation to overcome the defect acting as an obstacle is calculated depending on the material temperature, defect size, and interaction geometry. It is revealed that edge dislocations more efficiently absorb small loops than screw ones. It is demonstrated that, in the case of small loops, the number of reactions accompanied by loop absorption increases with temperature upon interaction with both edge and screw dislocations. It is established that Frank loops are stronger obstacles to the movement of screw dislocations than to the movement of edge ones.

DOI: 10.1134/S1027451014020062

INTRODUCTION

03X18H11 and 03X16H15M3 austenitic steels (their foreign analogs are, respectively, 304L and 316L steels), as well as 08X18H10T steel, are being actively used as structural materials in a number of components of nuclear reactors. For example, the upper block (covering, actuator, and mechanical assembly) of a series-produced WWER-1000 power reactor, protective tube block (its weight is ~60 t), and reactor cavity are manufactured from 08X18H10T steel. Although, austenitic steels initially exhibits good operating characteristics (strength, plasticity, corrosion stability, etc.), their properties degrade due to radiation-induced hardening and embrittlement during operation. This is caused by the accumulation and growth of radiation-induced defects arising from the action of a fast neutron beam on a material [1, 2]. As a rule, these processes are physically related to the interaction of extended radiation-induced defects with mobile dislocations because the defects are obstacles located in the glide planes of dislocations and, consequently, lead to an increase in the yield stress of a material [2].

It was demonstrated in several experimental works (see, e.g., review [3] and [4–6]) that, in austenitic steels, the predominant type of extended defects are interstitial Frank loops at a neutron irradiation dose of ~1 dpa (displacements per atom) and temperatures of less than $0.3T_m$ (T_m is the melting point). Frank loops, which correspond to an edge dislocation closed in a loop with an interstitial stacking fault along the extra plane, enter into reactions with mobile dislocations which determines the degree of hardening of an irradiated material. In particular, when loops are absorbed by dislocations, regions without radiation-induced defects are generated. This mechanism causes the appearance of inhomogeneous regions in the material, which, in turn, induce localized plastic deformation, giving rise to premature embrittlement of the material [7].

Since experimental investigations of irradiated materials are cumbersome and expensive, numerical simulation and prediction methods are finding wide applications. In particular, simulation performed on the atomic distance scale is considered a promising way of gaining additional information on the mechanisms by which irradiation affects properties of materials [8, 9]. With recent advances in computational capabilities, the classical molecular dynamics (MD) method is applicable to rather large model crystals with sides of several tens of nanometers. As a result, it is possible to reproduce typical Frank-loop sizes, the values of which are several nanometers [3–5], and the dislocation and defect densities in reactor materials and, moreover, to vary external load conditions [2, 9] in the numerical experiment. In the last few years, the majority of studies has been devoted to α iron and its alloys with body-centered cubic (BCC) lattices. Hence, their results are inapplicable to austenitic

alloys which have face-centred cubic (FCC) lattices. Recently, there have been a number of works wherein the MD method was employed to examine the interaction between dislocations and radiation-induced defects in pure metals (aluminum, nickel, and copper) with FCC lattices [10–13]. For example, in [10], the interaction of screw and edge dislocations with Frank loops 6 nm in diameter was investigated in copper at a temperature of $T = 600$ K. Two typical mechanisms of interaction with edge dislocations have been revealed: loop shifting and loop absorption giving rise to the formation of a superjog with a constriction. Note that the character of interactions depends substantially on the stacking-fault energy (SFE) and the elastic constant of materials. For example, the SFE of pure Cu is ~44 mJ/m^2, and the shear modulus is ~41 GPa. In contrast to pure FCC metals, austenitic alloys have appreciably lower SFEs (~20 mJ/m^2) and high shear moduli G (~80 GPa). Thus, the previously found dislocation–defect interaction mechanisms of pure FCC metals cannot be extrapolated to austenitic alloys, for which low SFE must be taken into account.

In the recently published work [14], the concept of atomistic simulation was used to analyze the mechanisms behind the interaction of edge and screw dislocations with Frank loops (4 nm in diameter) in a FCC Fe–Ni alloy at two Ni concentrations (50 and 70%) and in pure nickel. The Fe–Ni_{50} alloy is characterized by a combination of low SFE (~20 mJ/m^2) and a relatively high value of G (80 GPa). Such a combination of parameters is also inherent to austenitic alloys. As was established, constriction formation at dislocations is suppressed if the SFE decreases from 125 (pure Ni) to 50 mJ/m^2 (Fe–Ni_{70} alloy). As a result, the loop is sheared rather than conversion of the Frank loop into a perfect one (i.e., the stacking fault is removed). A significant disadvantage of the Fe–Ni model alloy is the strong dependence of the SFE on the nickel concentration, which, in turn, gives rise to strong sensitivity of the dislocation–defect interaction mechanisms under variations in local atomic environment near the defect.

To eliminate this disadvantage, the authors of [15] pioneered atomistic simulation of the interaction between screw dislocations and Frank loops in a ternary model alloy (Fe–Ni_{10}–Cr_{20}) with properties intrinsic to those of austenitic steels (03X18H11 and others), the main alloying components of which are nickel (~10%) and chromium (~20%). In this study, the new interatomic interaction model, which makes it possible to predict the correct relation of quantities SFE and G (typical of austenitic steels) in the Fe–Ni_{10}–Cr_{20} model alloy, was applied to the Fe–Ni–Cr system [16].

This work is the continuation of previous investigations [15] and is intended to analyze atomic mechanisms underlying the interaction between edge dislocations and Frank loops (2–5 nm in diameter) in the Fe–Ni_{10}–Cr_{20} model alloy at temperatures of T = 300–900 K, estimate the critical stresses required for an edge dislocation to overcome an obstacle, and compare calculations with the results [15] obtained for screw dislocations.

SIMULATION TECHNIQUE

In this work, the simulation technique is analogous to the procedure described comprehensively in [15]. Hence, only its basic aspects are indicated below. The classical MD method [17] using the many-body potential of interatomic interaction [16] based on the embedded atom model [18] is employed. The interatomic potential [16] was specially developed and optimized so as to implement atomistic simulation of the mechanical properties of the Fe–Ni_{10}–Cr_{20} model alloy with the FCC crystal lattice, low SFE, and high G.

Atomistic simulation was performed within the scope of the periodic dislocation model [19]. The model crystal consisted of ~1.5 million atoms, and its sizes were $113.1a_0 \times 121.9a_0 \times 27.7a_0$, where a_0 is the lattice constant. Periodic boundary conditions were applied along the X and Y axes ([110] and [1 $\bar{1}$ 2] directions, respectively). The (111) planes of the box faces were free surfaces perpendicular to the Z axis, and atoms of the few uppermost and lowermost (111) planes were rigidly fixed in their positions. The external load was implemented by shifting several upper (111) atomic planes of the model crystal. The external-load rate (due to shifting) was 30×10^6 s^{-1}, corresponding to a dislocation velocity of ~50 m/s. The total shear stress arising from the shifting of the upper crystal layers was determined by calculating the force acting on the lower fixed layer of atoms in the direction of applied load.

It was assumed that an edge dislocation with the 1/2[110] Burgers vector moves in the $(\bar{1}11)$ glide plane of the crystal containing an interstitial Frank loop with the 1/3[111], 1/3 [11 $\bar{1}$] or 1/3 [1 $\bar{1}$ 1] Burgers vectors and the (111), (11 $\bar{1}$) or (1 $\bar{1}$ 1) location planes, respectively. The interactions between a dislocation and a Frank loop were investigated under the condition that the dislocation slid along the opposite [$\bar{1}$ $\bar{1}$ 0] and [110] directions.

The dislocation density was 2.571×10^{15} m^{-2}. The diameters of the examined loops incorporating 55 and 367 interstitial atoms were 2 and 5 nm, respectively. According to the geometric sizes of the simulated box, the loop density is 6×10^{22} m^{-3}. Such loop diameters and density are typical for Frank loops observed experimentally in austenitic steels at irradiation doses of ~1 dpa [4, 5].

The final atomic configuration was analyzed using several criteria: the coordination number, the number of nearest neighbors of an atom corresponding to the FCC structure, and the potential energy of an atom. The atoms shown in the figures presented below have less than 12 neighbors whose local configuration corresponds to the FCC structure. Dislocation core atoms

Table 1. Yield stresses calculated when edge and screw dislocations move in the $Fe–Ni_{10}–Cr_{20}$ alloy without radiation-induced defects at different temperatures

Temperature, K	Yield stress, MPa	
	screw dislocation	edge dislocation
300	97	147
600	56	80
900	37	57

were assumed to be surrounded by 10 or 11 FCC neighbors, and a stacking fault was represented as a double layer of atoms, each having nine FCC neighbors.

The maximum applied loads at which a moving dislocation can overcome a Frank loop, σ_{max}, were determined by analyzing the averaged instantaneous load stresses $\sigma(t)$. The time interval of $\sigma(t)$ averaging was 500 fs.

RESULTS AND DISCUSSION

Numerical simulation based on the MD method was employed to determine the yield stresses σ_Y under the condition that edge and screw dislocations with the 1/2[110] Burgers vector move in a perfect crystal (i.e., without faults) at temperatures varying from 300 to 900 K. The yield stresses, which were calculated by averaging the resulting shear stresses over 2 ns, are presented in Table 1. It is seen from Table 1 that the quantity σ_Y is inversely proportional to temperature. At all temperatures under consideration, the yield stresses of moving edge dislocations exceed those of screw dislocations by a factor of 1.5.

For model crystals with Frank loops, 36 dislocation reactions between an edge dislocation having the 1/2[110] Burgers vector, which is split into partial dislocations with the 1/6[211] and 1/6 $[12\bar{1}]$) Burgers vectors and moves in the $(\bar{1}11)$ glide plane, and Frank loops having the 1/3[111], 1/3 $[11\bar{1}]$, and 1/3 $[1\bar{1}1]$ Burgers vectors were investigated at temperatures of $T = 300$, 600, and 900 K along two possible ($[\bar{1}\,\bar{1}0]$ and [110]) directions of approach.

It was ascertained that, according to the interaction type, all dislocation reactions can be divided into five main categories.

1. Half-Loop Absorption by a Dislocation and the Formation of a Superjog with a Constriction

1a. Under the action of external load, partial dislocations slide toward a loop and a leading dislocation (LD) approaches the loop (Fig. 1a). Owing to the further application of stresses, the right segment of the LD undergoes bending (left (L) and right (R) orientations are shown in Fig. 1a and used in descriptions of subsequent reactions) and its screw-shaped region is observed near the loop (Fig. 1b). The left segment of the edge dislocation accumulates elastic stress, which is suppressed by the nucleation of two Shockley partials (in the place where the segment is attached to the loop). As a result, the interstitial stacking fault of the lower half-loop is eliminated and the right segment of the lower half-loop slides along the screw-shaped segment of the right part of the LD (Fig. 1c). Thereafter, under the action of applied stress, a junction is formed in the region where the LD right segment is attached to the half-loop and the given segment detaches. The LD left segment and tailing dislocation (TD) remain attached to the half-loop. The subsequent application of external load is associated with the fact that the lower part of the half-loop moves forward along the LD left segment and the TD, and leading and tailing dislocations are detached from the remaining half-loop. As a result, a superjog with a constriction is generated at the dislocation, and a half-loop with an unchanged Burgers vector is located behind the dislocation (Fig. 1d).

1b. When the temperature is $T = 600$ K, the loop diameter is 5 nm, the Burgers vector of the loop is [111], and the dislocation moves along the $[\bar{1}\,\bar{1}0]$ direction, a pair of Shockley partials arises in the upper half-loop at the instant of junction formation (Fig. 1b), fol-

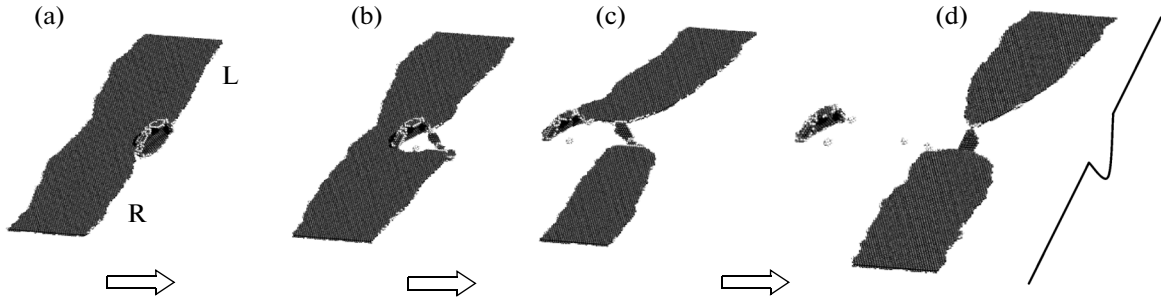

Fig. 1. Visualization of dislocation reaction 1a characterizing the interaction between the edge dislocation moving along the $[\bar{1}\,\bar{1}0]$ direction and the Frank loop (5 nm in diameter) with the Burgers vector $\boldsymbol{b_L} = 1/3[111]$ at the temperature $T = 300$ K and within (a) 185, (b) 290, (c) 395, (d) 520, and (e) 640 ps after the beginning of simulation.

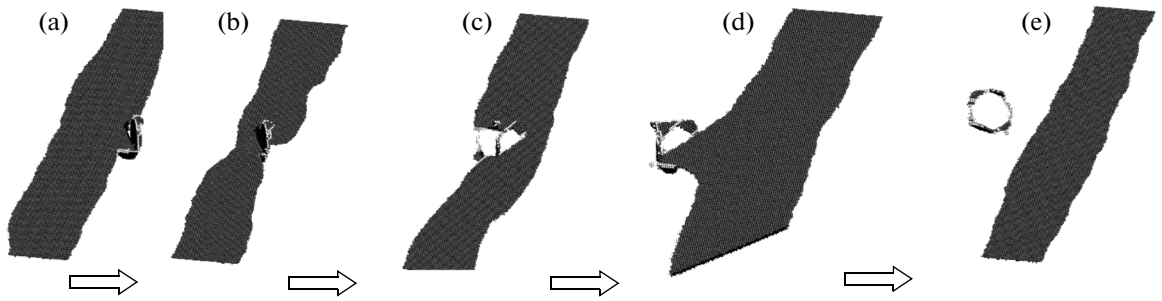

Fig. 2. Visualization of dislocation reaction 2 characterizing the interaction between the edge dislocation moving along the [110] direction and the Frank loop (5 nm in diameter) with the Burgers vector $\boldsymbol{b_L} = 1/3\,[1\,1\,\bar{1}]$ at the temperature $T = 600$ K and within (a) 120, (b) 255, (c) 265, (d) 540, and (e) 905 ps after the beginning of simulation.

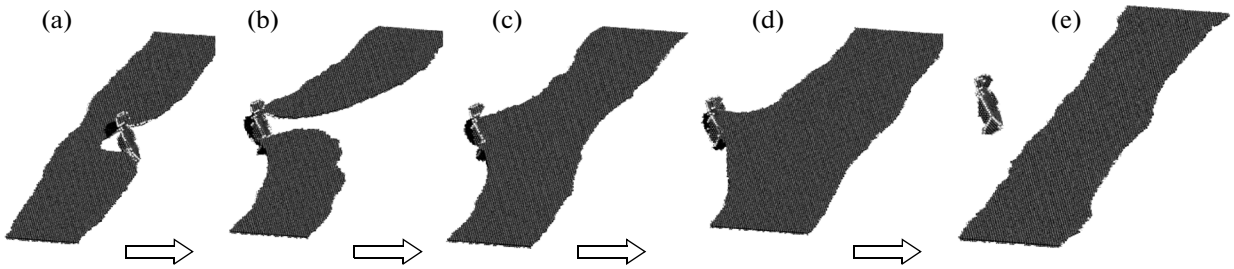

Fig. 3. Visualization of dislocation reaction 3a characterizing the interaction between the edge dislocation moving along the $[\bar{1}\,\bar{1}0]$ direction and the Frank loop (5 nm in diameter) with the Burgers vector $\boldsymbol{b_L} = 1/3\,[1\,1\,\bar{1}]$ at the temperature $T = 600$ K. The shown configurations were obtained at (a) 250, (b) 510, (c) 515, (d) 585, and (e) 910 ps after the beginning of simulation.

lowed by stacking-fault removal. After completion of detachment of the leading and tailing dislocations, a superjog with a constriction appears at the dislocation (by analogy with the case shown in Fig. 1d) and a perfect dislocation loop with the 1/2[101] Burgers vector is created.

2. Loop Conversion into a Perfect Configuration due to the Stacking-Fault Elimination Followed by Constriction Formation

The LD is attracted to the loop (Figs. 2a, 2b) and a constriction is generated on the LD right segment in the place of its attachment to the loop. Since Shockley partials arise in the loop, the stacking faults of the entire loop are eliminated. Thereafter, the LD moves forward and the TD remains fastened to the loop. The upper segment of the loop is resplit so that a "bridge" with the TD is formed along the applied stress direction (Fig. 2c). This bridge disappears when the TD separates from the loop (Fig. 2d). Due to this reaction, a perfect dislocation loop with the 1/2[011] Burgers vector is created. When the temperature was $T =$ 900 K, the $[1\,1\,\bar{1}]$ Burgers vector was used, and the dislocation slid along the [110] direction, the aforementioned bridge was not formed.

3. Loop Shifting Followed by the Closure of a Screw-Dislocation Dipole

During these reactions, the LD left and right segments attached to the loop bend so that a screw-dislocation dipole is generated and then is annihilated because the Burgers vectors of the two segments of the dipole have opposite signs.

3a. Reaction accompanied by constriction formation. When approaching a loop, the LD is repelled by the stacking fault of the loop (Fig. 3a).The LD left segment becomes attached to the loop, creates a constriction, and bends forward (Fig. 3b). At the same time, the right dislocation segment bends forward as well. The resulting screw-dislocation segment is annihilated, combining the LD left and right segments (Figs. 3c, 3d). Further application of load is characterized by the fact that the TD detaches from the loop (Fig. 3e). When the loop size is 5 nm, the temperature is 900 K, the $[1\,1\,\bar{1}]$ Burgers vector is used, and the dislocation slides along the $[\bar{1}\,\bar{1}0]$ direction during the given reaction, a pair of Shockley dislocations appear inside the loop at the instant of detachment from the TD and eliminates its stacking fault. The resulting perfect loop has the $1/2[0\,1\,\bar{1}]$ Burgers vector.

3b. Reaction accompanied by constriction formation. This reaction is similar to type 2a. The only dif-

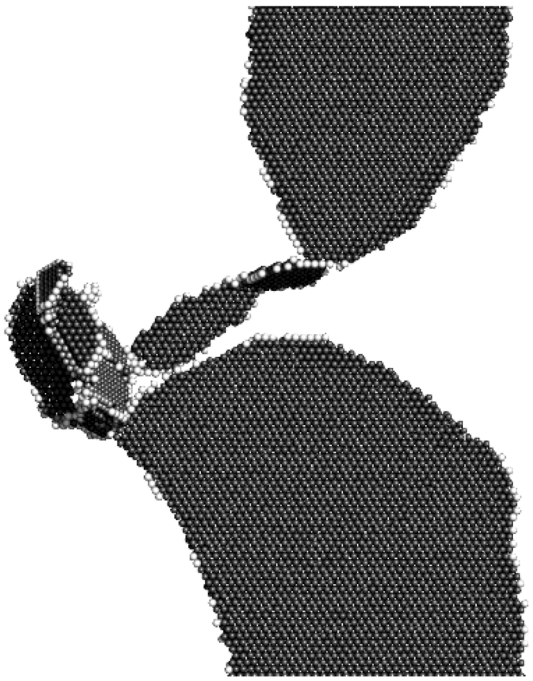

Fig. 4. Visualization of the configuration observed before the dislocation dipole collapse during reaction 3b characterizing the interaction between the edge dislocation moving along the $[\bar{1}\,\bar{1}0]$ direction and the Frank loop (5 nm in diameter) with the Burgers vector $\boldsymbol{b_L} = 1/3\,[11\,\bar{1}]$ at the temperature $T = 300$ K and 570 ps after the beginning of simulation.

ference is that the constriction slides along the loop edge starting at the instant shown in Fig. 3b. Hence, the left dislocation segment is partially resplit in the adjacent {111} planes (Fig. 4). The dipole closure mechanism and the reaction outcome are analogous to those observed in reaction 3a. For the given reaction, in which the loop size is 2 nm, the temperature is 600 K, the [111] Burgers vector is used, and the direction of dislocation motion is [110], a pair of Shockley partials is generated in the loop at the instant of TD detachment from the loop and removes its stacking fault. The Burgers vector of the formed perfect loop is 1/2[101].

3c. Reaction without constriction formation. Under the action of applied stress, the LD approaches a loop and becomes joined to its edges, repelling from the stacking fault of the loop (Fig. 5a). The subsequent application of load gives rise to bending of the LD left and right segments (Fig. 5b) and the formation of a dipole of screw dislocations which is annihilated (Fig. 5c). Thereafter, the LD moves forward (Fig. 5d), and the TD first attaches to the loop and then detaches from it (Fig. 5e). Owing to TD separation from the loop (Fig. 5d), several configurations of the given interactions exhibited the following features: the lower half-loop was absorbed and a superjog was formed when the loop size was 2 nm, the temperature was 600 K, the Burgers vector was [111], and the dislocation moved along the $[\bar{1}\,\bar{1}0]$ direction. At the instant of TD detachment from the loop, the latter was absorbed by the dislocation and two mutually repelling superjogs appeared on the TD under the condition that the loop size was 2 nm, the temperature was 900 K, the [111] Burgers vector was used, and the direction of dislocation motion was [110]. At the instant of separation from the TD, the stacking fault was removed due to the appearance of a pair of Shockley partials and, consequently, Frank-loop conversion into a perfect loop with the $1/2\,[01\,\bar{1}]$ Burgers vector when the loop size was 2 nm, the temperature was 900 K, the Burgers vector was $[11\,\bar{1}]$, and the direction of dislocation motion was $[\bar{1}\,\bar{1}0]$.

3d. Reaction without constriction formation. This reaction has an initial stage (Figs. 6a, 6b) resembling reaction 1a described above (Figs. 1a–1c). The difference is that the left and right segments of the dislocation bend forward without constriction formation (Fig. 6b). The lower loop segment begins to move forward along the LD left and right segments. A screw-dislocation dipole is created, is annihilated, and leaves an upper half-loop with the stacking fault behind (Fig. 6c). Further application of load causes the LD

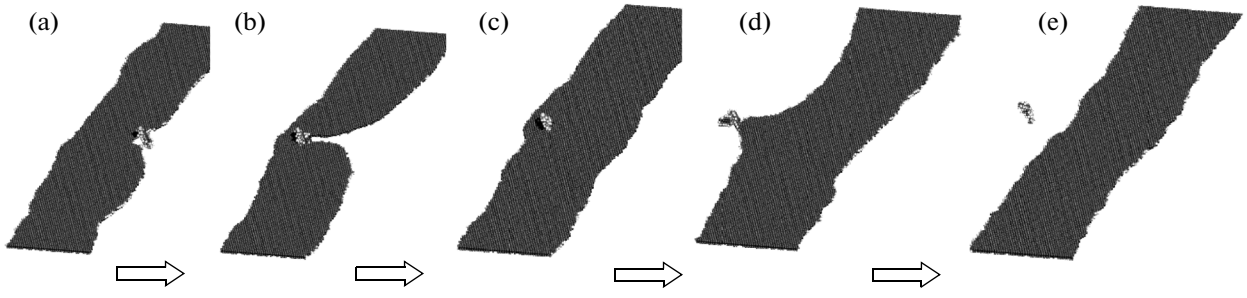

Fig. 5. Visualization of dislocation reaction 3c characterizing the interaction between the edge dislocation moving along the $[\bar{1}\,\bar{1}0]$ direction and the Frank loop (2 nm in diameter) with the Burgers vector $\boldsymbol{b_L} = 1/3\,[11\,\bar{1}]$ at the temperature $T = 300$ K. The shown configurations correspond to (a) 235, (b) 410, (c) 415, (d) 530, and (e) 925 ps after the beginning of simulation.

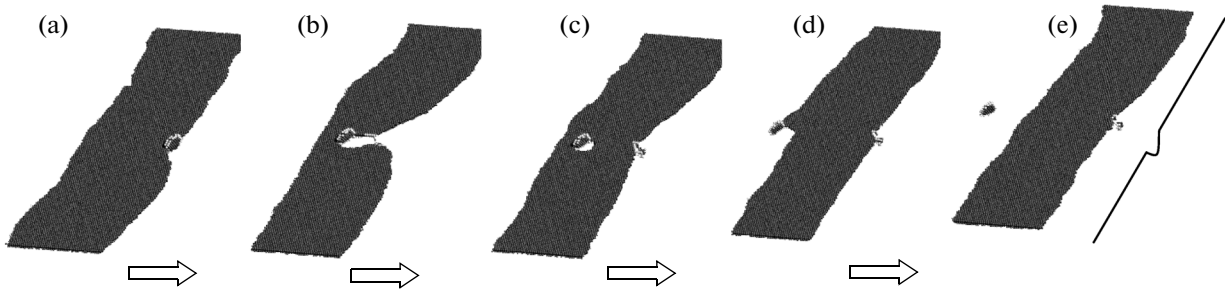

Fig. 6. Visualization of dislocation reaction 3d characterizing the interaction between the edge dislocation moving along the $[\bar{1}\,\bar{1}0]$ direction and the Frank loop (2 nm in diameter) with the Burgers vector $\boldsymbol{b_L} = 1/3[111]$ at the temperature $T = 900$ K. The shown configurations correspond to (a) 165, (b) 330, (c) 340, (d) 440, and (e) 530 ps after the beginning of simulation.

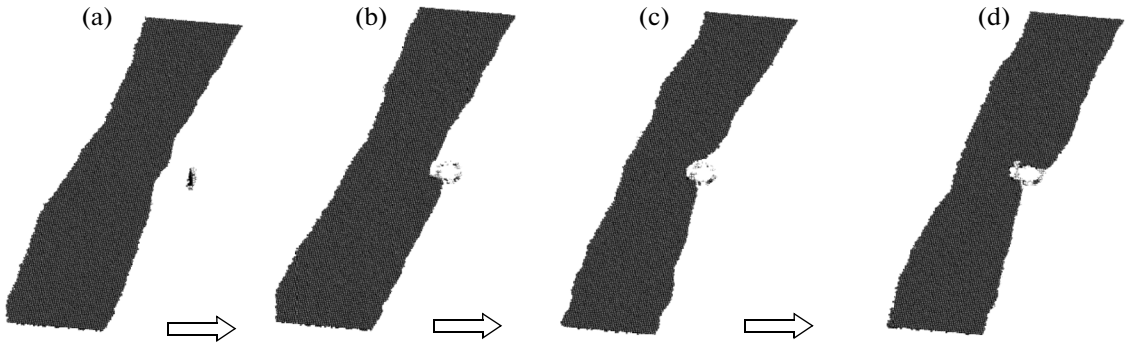

Fig. 7. Visualization of dislocation reaction 5a characterizing the interaction between the edge dislocation moving along the [110] direction and the Frank loop (2 nm in diameter) with the Burgers vector $\boldsymbol{b_L} = 1/3\,[1\,1\,\bar{1}]$ at the temperature $T = 900$ K. The shown configurations correspond to (a) 70, (b) 80, (c) 185, and (d) 220 ps after the beginning of simulation.

with the superjog to slide forward while and the TD detaches from the loop (Figs. 6d, 6e).

4. Successive Loop Shifting by Leading and Tailing Partial Dislocations

During the given reactions, a screw-dislocation dipole was not formed. The LD approaches a loop and attaches to it (by analogy with the case shown in Fig. 6a). The applied loads induce LD detachment from the loop and TD motion toward it (by analogy with the case shown in Fig. 6b). However, the LD has time to detach before TD approach. Thereafter, the TD separates from the loop (by analogy with the case shown in Fig. 6d). Due to the reaction, the loop is shifted forward. For the given reaction, in which the loop size is 2 nm, the temperature is 900 K, the Burgers vector is $[1\,\bar{1}\,1]$, and dislocation motion is along the $[\bar{1}\,\bar{1}0]$ direction, the lower half-loop is absorbed with superjog generation on the LD, and the stress field of an incoming TD creates a pair of Shockley partials in the upper half-loop, which eliminates the stacking fault. The Burgers vector of the formed perfect loop is 1/2[101].

5. Frank-Loop Conversion into a Perfect Loop upon Dislocation Approach

5a. Loop absorption with the formation of one or two superjogs in the leading dislocation. Under the action of applied stress, the LD moves toward a loop (Fig. 7a). The stress field surrounding the LD stimulates loop attraction to the dislocation, which is accompanied by stacking-fault removal (Fig. 7b), i.e., its conversion into a perfect loop with the 1/2[011] Burgers vector. Thereafter, the perfect loop interacts with the LD so that the lower and upper half-loop are attached to the LD. As a result, the LD with the two half-loops continues to move forward (Figs. 7c, 7d). In the case where the reaction occurs at $T = 900$ K, the $[1\,1\,\bar{1}]$ Burgers vector, and the [110] direction of dislocation motion, it was found that the upper loop segment is split in the other {111} plane due to the application of load. Thereafter, the formed stacking fault of the upper half-loop segment is eliminated upon TD approach to the loop. Under the subsequent action of the load, the TD separates from the perfect loop with the [101] Burgers vector and the LD with a superjog continues its motion.

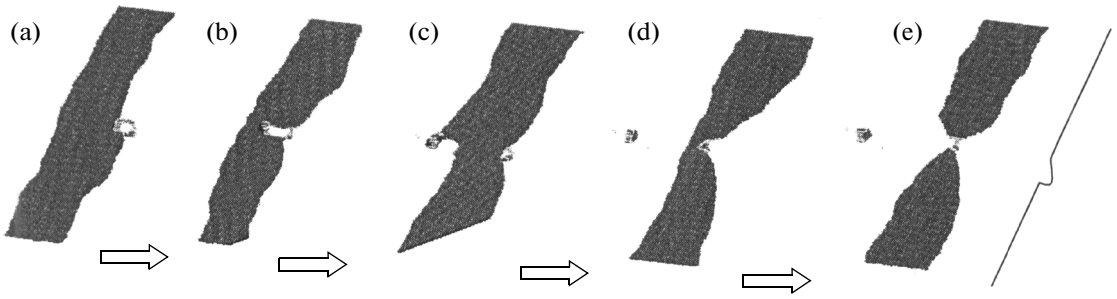

Fig. 8. Visualization of dislocation reaction 5b characterizing the interaction between the edge dislocation moving along the [110] direction and the Frank loop (2 nm in diameter) with the Burgers vector $\boldsymbol{b}_L = 1/3\,[11\,\bar{1}]$ at the temperature $T = 300$ K. The shown configurations correspond to (a) 125, (b) 350, (c) 565, (d) 870, and (e) 990 ps after the beginning of simulation.

5b. Half-loop absorption in the form of a superjog and the subsequent formation of a superjog with a constriction. Owing to the application of load, the LD moves toward a loop. The LD stress field induces loop attraction to the dislocation, which is accompanied by stacking-fault removal (Fig. 8a). Thereafter, the upper and lower loop segments become detached from each other, remaining joined to the LD (Fig. 8b). The latter continues to move after the lower half-loop segment is absorbed in the form of a superjog. In this case, the TD approaches the upper half-loop and then detaches from it (Fig. 8c). As a result, after the completion of TD detachment, a perfect loop with the 1/2[101] Burgers vector is observed (Fig. 8d). The stacking fault arising inside the lower half-loop decelerates dislocation motion. The approaching TD induces constriction generation followed by the appearance of a superjog with a junction on the dissociated dislocation, which continues to move forward (Fig. 8e).

For all 36 dislocation reactions discussed above, the maximum applied loads σ_{max} (after deduction of the corresponding yield stresses), which are necessary for the dislocations to penetrate through Frank loops 2 and 5 nm in diameter, are depicted, respectively, in Figs. 9a and 9b, where the stresses of detachment from screw dislocations are presented with allowance for the corrected yield stresses and the increased averaging time (see above). The averaged (over all specified types of reactions) values of σ_{max}, which were determined at two loop sizes and different temperatures, are presented in Table 2.

Table 2. Maximum applied stresses (after subtraction of the yield stress) in megapascals. Data were averaged over the reaction type and correspond to edge dislocation passage through Frank loops at different values of loop size D and temperature

Temperature/reaction type		300 K	600 K	900 K
$D = 2$ nm	3	80	96	64
	4	55	69	85
	5	71	55	40
$D = 5$ nm	1	101	84	85
	2	–	155	77
	3	162	163	146
	4	113	94	79

As is seen from the diagrams in Fig. 9, Frank loops are more complex obstacles for moving screw dislocations than for edge ones. In the case of screw dislocations, small values of σ_{max} correspond to the reaction according to which a loop is absorbed at a dislocation in the form of a helical turn [15]. This is related to the fact that this turn cannot move in the glide plane. In the case of an edge dislocation, the given reaction was not observed. For the two types of dislocations, the reactions accompanied by the bending of the left and right segments of a dislocation and the closure of LD segments due to the coalescence of forming screw and edge dipoles (reactions with edge and screw dislocations, respectively). The closure of edge- and screw-dislocation dipoles requires the application of different stresses. In the case of screw dislocations [2], their values are higher, thereby explaining the higher detachment stress in the implementation of similar reactions.

In the case of screw dislocations, almost two-thirds of the examined reactions (eleven with a loop size of 2 nm, and eleven with a size of 5 nm) were associated with loop shifting (without its absorption or conversion into a perfect loop). At the same time, in the case of edge dislocations, loop shifts were observed in half of the reactions (eight with a loop diameter of 2 nm, and ten with a diameter of 5 nm). It should be noted that, only in the case of the reactions of interaction between screw and edge dislocations and loops 2 nm in diameter, an increase in temperature decreases the portion of reactions accompanied by the loop shifting. For edge dislocations, the reactions corresponding to screw dislocations (except for the loop shifting) were not implemented. Instead, reactions by which a dislocation absorbs a loop to form a superjog with a constriction, a loop is absorbed with the formation of one or several superjogs at the leading or tailing disloca-

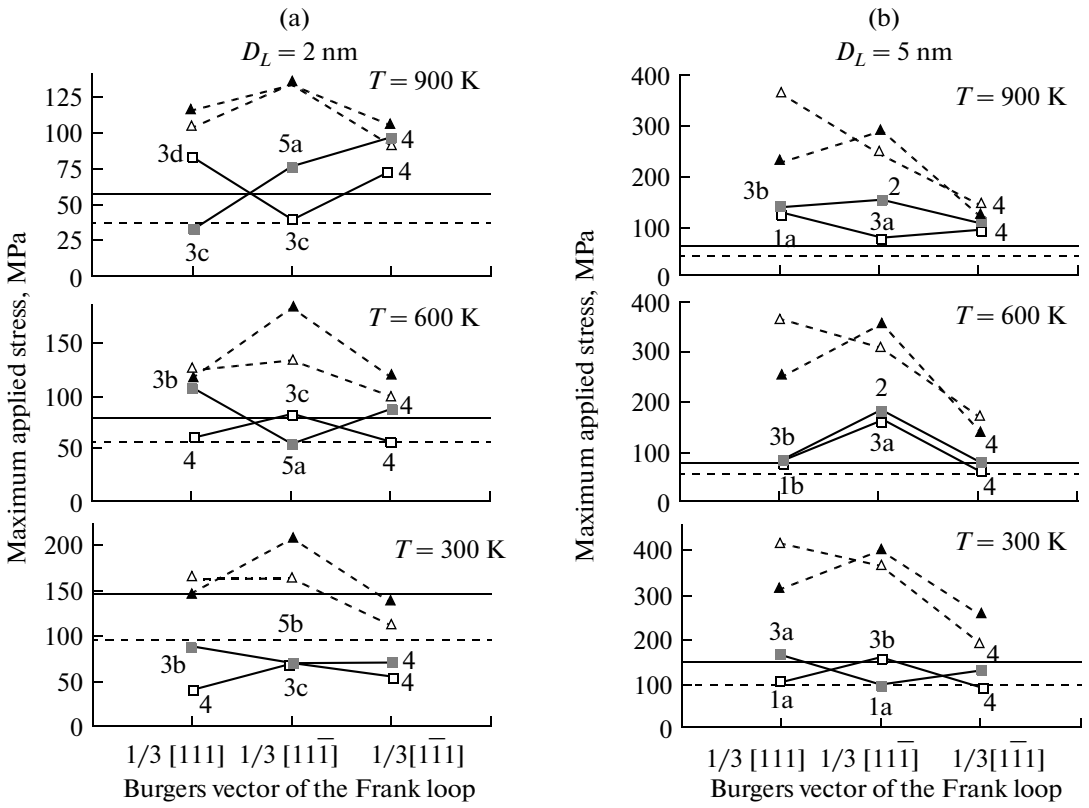

Fig. 9. Diagrams of the maximum applied load stresses (after subtraction of the yield stress), which are necessary for screw and edge dislocations (shown in black and white, respectively) to penetrate through Frank loops (a) 2 and (b) 5 nm in diameter, vs. the material temperature, Burgers vector, and direction of dislocation motion. Open and filled marks designate dislocation motions along the [$\bar{1}\,\bar{1}$0] and [110] directions, respectively. Numerals near each mark correspond to the type of the dislocation–Frank loop interaction. The yield stresses σ_Y are shown at each given temperature: solid and dashed lines designate the edge and screw dislocations, respectively.

tions, or a loop converts into a perfect one (before contact between a dislocation and a loop) were observed.

Let us restrict ourselves by consideration of the interaction between edge dislocations and Frank loops. Then, it is obvious from the diagrams in Fig. 9 and Table 2 that the reaction type depends (in particular) on the loop size. In the case of small loops (2 nm in diameter), there were no reactions 1 and 2, which were accompanied by either half-loop absorption and the generation of a superjog with a constriction or loop conversion into a perfect loop due to stacking-fault removal with constriction and bridge formation. These reactions were observed only if the loop diameter was 5 nm. Reaction 5, in which a Frank loop is converted into a perfect loop during dislocation approach (when the loop is surrounded by a dislocation stress field), occurred only if the loop diameter was small (2 nm).

For large loops (5 nm in diameter), the largest possible detachment stress corresponds to reactions 3 (the appearance and closure of a dislocation dipole), and the lowest value, to reactions 1 accompanied by half-loop absorption in the form of a superjog with a constriction. In the case of small loops, the maximum detachment stress is observed in reactions 3 (the formation and closure of a dislocation dipole) at temperatures of 300 and 600 K and in reaction 4 (successive shifting of leading and tailing partial dislocations) at a temperature of 900 K. The minimum detachment stress corresponds to reaction 4 (at T = 300 K) and reactions 5 (at T = 600 and 900 K).

In the majority of cases, the reaction mechanism was determined by temperature at the same configurations of interaction. For example, the dislocation was not resplit in the other {111} planes when the dislocation moving along the [$\bar{1}\,\bar{1}$0] direction interacted with a Frank loop (5 nm in diameter) with the [101] Burgers vector at a temperature 300 K. However, this effect was observed at temperatures of 600 and 900 K. Note that only one reaction of six was the shifting of the loop 2 nm in diameter at a temperature 900 K. At the same time, three reactions of six were accompanied by loop shifting if the diameter was 5 nm.

As was demonstrated in [14], the reaction with loop shifting occurred if the edge dislocations interacted with loops with diameters of 4.0 and 4.5 nm in Fe–Ni50% alloy at T = 300, 600, and 900 K. In [10],

when an edge dislocation interacted with a Frank loop (6 nm in diameter) in Cu, two types of interactions were revealed: (i) loop shifting and (ii) loop absorption in the form of a superjog with a constriction. Thus, in the examined austenitic alloy containing loops with similar sizes, the loop–edge dislocation reaction mechanisms (except for the aforementioned reactions in [10, 14]), which are related to the appearance of a pair of Shockley partials in the loop-location plane, were found at the same temperatures. They correspond to the classical mechanism by which a Frank loop converts into a perfect loop, which was described in [2].

CONCLUSIONS

With the use of the $Fe–Ni_{10}–Cr_{20}$ model alloy, the mechanisms underlying the dislocation reactions between Frank loops and sliding edge dislocations have been analyzed and classified depending on the material temperature, loop sizes, and their orientation with respect to the dislocation. As a result, the following five basic types of reactions are revealed:

(i) Half-loop absorption at a dislocation with the formation of a superjog with a constriction.

(ii) Frank-loop conversion into a closed loop due to stacking-fault removal and constriction generation.

(iii) Loop shifting accompanied by the closure of a screw-dislocation dipole.

(iv) Successive loop shifting by leading and tailing partial dislocations.

(v) Loop conversion into a perfect loop upon the approach of a dislocation.

From the standpoint of the absorption of small loops (2 nm in diameter), edge dislocations are more efficient than screw ones. In the case where small loops interact with both edge and screw dislocations, an increase in the number of reactions accompanied by loop absorption is observed with increasing temperature.

The maximum external loads σ_{max} required for a dislocation to pass through a set of equivalent obstacles (Frank loops) are determined. It is demonstrated that Frank loops with sizes of 2 and 5 nm are stronger obstacles to moving screw dislocations than to moving edge ones. Hence, it can be inferred that just the interaction with screw dislocations contributes mainly to radiation-induced hardening. Moreover, since quantity σ_{max} depends on the temperature, direction of dislocation motion, and loop sizes, it is clear that the loop–dislocation interaction geometry, the probably inhomogeneous distribution of loops in the material, and its temperature play an important role in estimating the dislocation-loop contribution to the material hardening under mechanical tests.

The performed research into the interaction of edge dislocations with Frank loops (together with the results of previous investigations of the corresponding interactions with screw dislocations) enables us to select a set of microscopic parameters (the maximum stresses of dislocation detachment and the interaction reaction classification versus the temperature, loop sizes, and interaction geometry), which can be used to parameterize the macroscopic simulation methods for determining the deformation processes of an irradiated material (in particular, the discrete dislocation dynamics method [20]).

REFERENCES

1. G. S. Was, *Fundamentals of Radiation Materials Science: Metals and Alloys* (Springer, Berlin,Heidelberg, New York, 2007).
2. D. J. Bacon, *Introduction to Dislocations*, 4th ed. (Butterworth-Heinemann, 2001).
3. S. J. Zinkle, P. J. Maziasz, and R. E. Stoller, J. Nucl. Mater. **206**, 266 (1993).
4. C. Pokor and Y. Brechet, J. Nucl. Mater. **326**, 19 (2004).
5. C. Pokor and Y. Brechet, J. Nucl. Mater. **326**, 30 (2004).
6. V. S. Neustroev, Vopr. At. Nauki Tekh.: Ser. Fiz. Rad. Povrezhd. Rad. Materialoved., No. 6, 78 (2007).
7. Xiaoqiang Li and A. Almazouzi, J. Nucl. Mater. **385**, 329 (2009).
8. V. A. Kirsanov, *Computer Experiment in Nuclear Materials Science* (Energoatomizdat, Moscow, 1990) [in Russian].
9. D. Terentyev, D. J. Bacon, and Yu. N. Osetsky, Philos. Mag. **90**, 1019 (2010).
10. T. Nogaret, C. Robertson, and D. Rodney, Philos. Mag. **87**, 945 (2007).
11. D. Rodney and G. Martin, Phys. Rev. B **61**, 8714 (2000).
12. D. Rodney, Acta Mater. **52**, 607 (2004).
13. Y. N. Osetsky, D. Rodney, and D. J. Bacon, Philos. Mag. **86**, 2295 (2006).
14. D. Terentyev, A. Bakaev, and Yu. N. Osetsky, J. Nucl. Mater. **442** (Suppl. 1), S628 (2013).
15. A. V. Bakaev, D. A. Terentyev, E. E. Zhurkin, and P. Yu. Grigoriev, J. Surf. Invest.: X-Ray, Synchrotron Neutron Tech. **7**, 211 (2013).
16. G. Bonny, D. Terentyev, R. C. Pasianot, S. Poncé, and A. Bakaev, Model. Simul. Mater. Sci. Eng. **19**, 085008 (2011).
17. M. P. Allen and D. J. Tildesley, *Computer Simulations of Liquids* (Clarendon, Oxford, 1987).
18. M. S. Daw and M. I. Baskes, Phys. Rev. B **29**, 6443 (1984).
19. Y. N. Osetsky and D. J. Bacon, Model. Simul. Mater. Sci. Eng. **11**, 427 (2003).
20. S. Queyreau, G. Monnet, and B. Devincre, Acta Mater. **58**, 5586 (2010).

Translated by S. Rodikov